



UNIVERSITY OF LEEDS

This is a repository copy of *Oxygen, sulfur and selenium terminated single-walled heterocyclic carbon nanobelts (SWHNBs) as potential 3D organic semiconductors*.

White Rose Research Online URL for this paper:
<http://eprints.whiterose.ac.uk/129314/>

Version: Accepted Version

Article:

Jones, L orcid.org/0000-0001-6657-2632, Lin, L and Chamberlain, TW orcid.org/0000-0001-8100-6452 (2018) Oxygen, sulfur and selenium terminated single-walled heterocyclic carbon nanobelts (SWHNBs) as potential 3D organic semiconductors. *Nanoscale*, 10 (16). pp. 7639-7648. ISSN 2040-3364

<https://doi.org/10.1039/C8NR01216D>

© 2018, The Royal Society of Chemistry. This is an author produced version of a paper published in *Nanoscale*. Uploaded in accordance with the publisher's self-archiving policy.

Reuse

Items deposited in White Rose Research Online are protected by copyright, with all rights reserved unless indicated otherwise. They may be downloaded and/or printed for private study, or other acts as permitted by national copyright laws. The publisher or other rights holders may allow further reproduction and re-use of the full text version. This is indicated by the licence information on the White Rose Research Online record for the item.

Takedown

If you consider content in White Rose Research Online to be in breach of UK law, please notify us by emailing eprints@whiterose.ac.uk including the URL of the record and the reason for the withdrawal request.



eprints@whiterose.ac.uk
<https://eprints.whiterose.ac.uk/>

Oxygen, sulfur and selenium terminated single-walled heterocyclic carbon nanobelts (SWHNBs) as potential 3D organic semiconductors

L. Jones¹ L. Lin¹ and T. W. Chamberlain^{2*}

¹Centre for Industrial Collaboration, School of Chemistry, University of Leeds, UK, LS2 9JT

²Institute of Process Research and Development, School of Chemistry, University of Leeds, LS2 9JT

Abstract

Carbon nanomaterials such as polyaromatic hydrocarbons (PAHs), graphene, fullerenes and nanotubes are on the frontline of materials research due to their excellent physical properties, which in recent years, have started to compete with conventional inorganic materials in charge transfer based applications. Recently, a variety of new structures such as single-walled carbon nanobelts (SWCNBs) have been conceived, however, to date only one ‘all-phenyl’ example has been synthesised, due to problems with their stability and the challenging synthetic methodologies required. This study introduces a new class of phenacene-based SWCNBs and their chalcogenide derivatives, forming the new sub-class of single-walled heterocyclic carbon nanobelts (SWHNBs) which are expected to be both more stable and easier to synthesis than the all carbon analogues. Subsequent theoretical examination of the structure-property relationships found that unlike the small-molecule acene homologues (tetracene, pentacene *etc.*) which become more reactive with addition of oxygen, an increase in the molecular size of the SWCNBs actually stabilises the HOMO energy level, in correlation with the increasingly negative nuclear independent chemical shift (NICS) calculations of their cylindrical aromaticities. Interestingly, the FMO energies of the phenacene SWCNBs are similar to that of the nanobelt reported by Itami and co-workers, but those of the SWHNBs are deeper and thus more stable. Moreover, the sulfur derivative of one SWHNB was found to give hole-charge transfer mobilities as high as $1.12 \text{ cm}^2 \text{ V}^{-1} \text{ s}^{-1}$, which is three orders of magnitude larger than the corresponding unsubstituted SWCNB ($3 \times 10^{-3} \text{ cm}^2 \text{ V}^{-1} \text{ s}^{-1}$). These findings suggest the candidates are air-stable and are high-performing organic semiconductors for organic thin film transistor (OTFT) devices, while the structure-property relationships uncovered here will aid the design and synthesis of future three-dimensional organic nanomaterials.

Introduction

The field of molecular carbon nanomaterials has been rekindled in light of the recent synthesis of an all-phenyl nanobelt by Itami and co-workers¹ in 2017. Nanobelts are aromatic hydrocarbon structures consisting primarily of fused benzene rings in a belt-like array (Figure 1). In essence, these are the smallest possible slice of a carbon nanotube yet pertain to have high semiconducting properties. Such nanomaterials are desirable in transistor technology, due to their varied properties such as low band gaps for transistor devices²⁻⁴ and singly-occupied orbitals for spintronics^{5,6}; their size also enables very high

transistor density per unit area⁷⁻¹⁰, which results in improved power control in electronic devices. Structures that have been synthesised include a cyclophenylene, a functionalised C₆₀ and a mixed benzene and octacene belt have showed that a fused-ring phenyl belt should be possible^{11,12}. Many attempts in the past have tried but ultimately failed to yield this desirable product, owing largely to the unstable intermediates and challenging reaction conditions required. Now however, the work by Itami’s group show such molecular structures are not only possible, but could lead to a new revolution in organic materials discovery¹³⁻¹⁷.

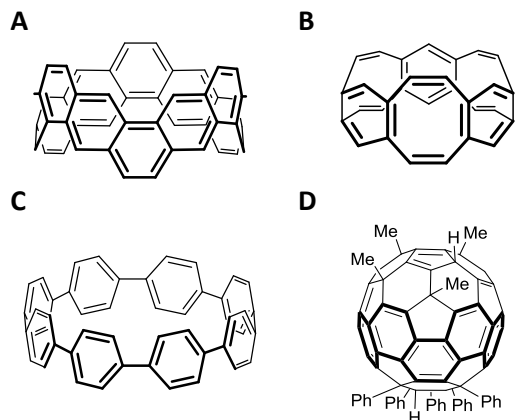


Figure 1. (A) The first single-walled all-phenyl carbon nanobelt by Itami and co-workers in 2017, a mixed zig-zag and chair structure; (B) a mixed phenyl and octyl belt; (C) a cycloparaphenylene; and (D) a phenyl belt from a derivatised C_{60} .

The structure of Itami's nanobelt is neither chair nor zig-zag in nature, but a mixture of both due to the derivatised asymmetric para-xylene starting reagents and successive Wittig coupling reactions. This synthesis of this molecule will undoubtedly unlock new synthetic routes not yet foreseen, but what is not available with this structure is the ability to tune its physical properties through width and edge modification¹⁸, which would open up the potential applications in organic electronics. One way to induce atomically-precise structures with discrete properties, is the rational design of the nanomaterial structure with heteroatoms sitting along the terminus, akin to those of heteroacene^{19–23} and heterocirculene²⁴ materials. However, it is currently difficult to consider how Itami's carbon nanobelt can be further derivatised in its current form, something which is essential as derivatisation will be important to enable the properties of nanobelts to be fully realised. Indeed, "Sulflower" was synthesised in 2006 by Chernichenko²⁵ and yet there has been no reports of non-planar analogues in a belt-like form to date. Knowledge of these structures are still limited and are

largely acquired through computational chemistry calculations⁶.

The development of a detailed understanding of structure-property relationships will help current and future synthetic efforts, particularly for the selection of the target and device combinations in organic transistors and photovoltaics. A comparison of the carbon backbones of the nanobelts and heterocirculenes gives the realisation that the chair form is key for two reasons: (1) the construction of a five-membered heterocyclic derivative needs four other members, normally carbon atoms arranged in a cis-diene array; (2) chair conformers lead to phenacene belts, which have the four-membered carbon backbone available for substitution. It is natural then, to consider the potential for heteroacene belts, or rather, single-walled heterocyclic carbon nanobelts (SWHNBs) as illustrated in Figure 2. Such structures would benefit from structural and atomic stabilising factors, while providing whole new sub-classes to explore and tune their physical-properties for high-performing molecular materials in organic electronics. Herein, we propose a new class of carbon oxygen, sulfur, and selenium SWHNBs. This work begins by exploring their aromaticities, probes their stabilities and then investigates their charge transfer properties for applications as organic semiconductors in organic thin-film transistors (OTFTs).

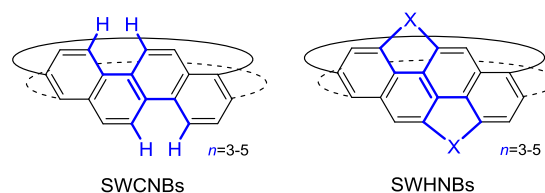


Figure 2. General structures of chair-SWCNBs (left) and the SWHNBs in this work (right); the repeat unit is highlighted in blue ($X = O, S, \text{ or } Se$).

Computational Methods

Avogadro²⁶ (version 1.1.1) and Chemcraft were used for both the construction of the molecules and the visualisation of their surfaces. All calculations were performed at the B3LYP/6-31+G(d)²⁷⁻²⁹ level in Gaussian 09³⁰ (version D.01); larger basis sets were computationally intractable due to the size of the polyatomic structures. The ground states were first optimized in Avogadro with the molecular mechanics universal force field (UFF), then optimized with quantum mechanics at the given theoretical level using density functional theory (DFT) in Gaussian 09; all subsequent single-point and vertical calculations were performed from the optimized structures at the same level of theory. All optimized structures were confirmed to be ground state with frequency calculations, *i.e.* no negative frequencies were observed (vibrational spectra are available in the ESI†).

The nature of their aromaticities were investigated with nuclear independent chemical shifts (NICS)³¹, susceptibility exaltations and the aromatic C=C vibrational stretch. NICS(0) are a measure of the total $\sigma+\pi$ electron delocalisation effects. The global and local NICS were calculated at the centre of each molecule (NICS_{MC}(0)) and at the centre of each benzene ring (NICS_{RC}(0)) in the phenacene belts, respectively, at the GIAO approximation³²⁻³⁴. The exaltation and NICS(0) result from the presence of cyclic delocalisation of ring currents. Significantly negative (*i.e.* magnetically shielded) NICS(0) and exaltation values observed at the centre of rings and/or at the centre of spherical molecules indicate the presence of diatropic ring currents or aromaticity, whereas the opposite is true for antiaromaticity. The NICS(0), exaltations and vibrations were calculate in Gaussian 09 with DFT. Although NICS uses virtual atoms, the shielding of He³ atoms in fullerene were found to compare well with experimental NMR values³⁵⁻

³⁸. Other methods to deduce aromaticity include homodesic reactions, bond-length alterations and stabilisation energies, however the constituents have to be chosen with care as they can be easily biased to give a desired result. With belt-like architectures, it is difficult to select molecular components that are similar in nature in terms of bond lengths, angles and strengths and thus these methods are not appropriate³¹.

Different theories were used to evaluate the vertical ionization energies and electron affinities and include DFT (B3LYP), Koopmans' Theorem (KT)³⁹⁻⁴¹ and a variant of the electron propagator theories such as the third-order pole (P3)^{42,43}. The charge-transfer properties were determined from the semi-classical Marcus-Hush Theory, such as the internal reorganization energy, the transfer integral and the rate of charge transfer. Marcus-Hush Theory⁴⁴ (Equation 1) describes the charge transfer as a self-exchange between a neutral and a charged (radical cation/anion) molecule. One key parameter, the internal reorganization energy⁴⁵ ($\lambda_{h,e}$), is intrinsic only to the extent of relaxation and upon which, the electron delocalisation plays a key part. Ideally, internal reorganization energies should be relatively small, *ca.* 100-200 meV⁴⁶.

$$k_{ct} = \left(\frac{t^2}{\hbar}\right) \left(\frac{\pi}{\lambda k_B T}\right)^{1/2} e^{\frac{-\lambda}{4k_B T}} \quad (1)$$

The energy processes of electron exchange, excitation and relaxation are illustrated in Figure. 3. The internal hole reorganization energy (λ_h) is comprised of two relaxation terms, the energy of the cationic (λ_1) and neutral (λ_2) surfaces, as defined in Equation 2. The cationic reorganization energy λ_1 is determined from the difference between the vertical and adiabatic ionization energies calculated via the vertical, single-point geometry of the cation (M^{+}_{SP}) and the optimized cation structure (M^{+}_{OPT}), (Equation 3).

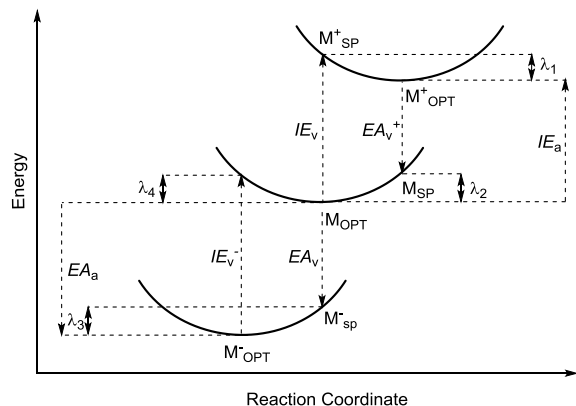


Figure 3. The ionization energy (IE) and electron affinity (EA) pathways between the anion, neutral and cation potential energy surfaces for the calculation of the hole (electron) reorganization energy $\lambda_h(\lambda_e)$.

$$\lambda_h = \lambda_1 + \lambda_2 \quad (2)$$

$$\lambda_1 = E(M_{SP}^+) - E(M_{OPT}^+) \quad (3)$$

Addition of an electron to the minimised cationic structure returns the molecule back to its neutral geometry and is performed with a vertical electron affinity of the cation, EA_v^+ ; the difference between this state and the minimum of the neutral molecule is λ_2 (Equation 4).

$$\lambda_2 = E(M_{SP}) - E(M_{OPT}) \quad (4)$$

Similarly, the internal electron reorganization energy λ_e , is calculated according to Equation 5, which is the difference of the constituent relaxations between the anionic (λ_3) and the neutral surfaces (λ_4), from Equations 6 and 7 respectively.

$$\lambda_e = \lambda_3 + \lambda_4 \quad (5)$$

$$\lambda_3 = E(M_{SP}^-) - E(M_{OPT}^-) \quad (6)$$

$$\lambda_4 = E(M_{OPT}^-) - E(M'_{SP}) \quad (7)$$

The transfer integral t_h is another important component in Marcus Theory and the hole

integral can be estimated from the “splitting-in-dimer” method^{27,47–49} (Equation 8), comprising of two cofacial molecules separated by a distance d (Å) and determined from calculating half the energy difference between the HOMO and HOMO-1 levels of the dimer. The electron transfer integral (t_e) is determined from the half difference between the energies of the LUMO+1 and LUMO states (Equation 9).

$$t_h = \frac{1}{2}(\Phi_H - \Phi_{H-1}) \quad (8)$$

$$t_e = \frac{1}{2}(\Phi_{L+1} - \Phi_L) \quad (9)$$

A range of dimer separations are appropriate to determine the extent of the electronic coupling interaction. A separation between $d = 3.3$ - 3.8 Å was experimentally found for planar OSCs^{27,49,50}, although this cannot be assumed for the novel structures in this study, as some are non-planar and will not have an identical packing arrangement. Therefore, the integrals were calculated with 0.5 Å increments between 3.0-5.0 Å inclusive. Substituting values for λ and t into Equation 1, enables the rates of hole and electron charge transfer ($k_{CT,h,e}$) to be determined at any given separation d . Marcus-Hush theory has a number of limitations which include a lack of entropy and nuclear tunneling, which have been incorporated, inter alia, with the Marcus-Levich-Jortner equation^{51,52} and that of McConnell’s⁵³. Although other charge transfer theories are available⁵⁴, the more simplified approach (Equation 1) which is still used widely in the literature^{27,55,56} and deployed in the present study, is suitable for *a priori* investigations on novel polyatomic compounds. Hole and electron mobilities (μ) were evaluated *via* the Einstein-Smoluchowski^{49,57} equation (10), where d is the intermolecular distance, k_{CT} is the rate of charge transfer, k_B is Boltzmann constant and T is temperature.

$$\mu = \frac{d^2 k_{CT}}{k_B T} \quad (10)$$

Results and Discussion

The chair-SWCNBs and SWHNBs are illustrated in Figure 4, showing the top and side views for each derivative ($n = 3-5$). Naturally, as the repeat unit increases from 3 to 5, the molecular dimensions such as the diameter and volume also increase (see ESI†). Molecules with a repeat unit of 2 would result in a cubane-like structure, which would have large ring strain and in practical terms be very difficult to synthesise.

The overall chemical formula for the SWCNBs is $C_{2n}H_n$ and for the SWHNBs is $C_{4n}X_n$, (where $X = O, S$ or Se). The SWCNBs are a tubular shape, while the SWHNBs are quasi-spherical. This may be due to the C-X-C bond angles, where those of oxygen **4-6**, sulfur **7-10** and selenium **10-12** are 105.5° , 89.4° and 64.6° respectively for the $n = 5$ species. To compensate for the large bonding angle of oxygen, the carbon atoms in **4-6** make use of the internal cavity space and lean inwards to satisfy the C=C bond lengths and angles around the phenyl rings.

The nature of the nanobelts aromaticities were probed with magnetic susceptibility exaltations (Λ), nuclear independent chemical shifts (NICS(0)) and the aromatic C=C vibration (Table 1). The mass-centred NICS_{MC}(0) values show correlation between aromaticity and molecular size. For example, the NICS_{MC}(0) value of the underivatized SWCNB **1** is positive (2.36 ppm), suggesting this structure is either nonaromatic or antiaromatic. However, those of **2** and **3** are increasingly negative at -4.43 ppm and -5.82 ppm respectively, which implies these two structures are indeed aromatic³³ and the extent of the aromaticity for the SWCNBs increases with molecular size. The same trend in NICS_{MC}(0) is observed with the sulfur (from -8.77 to -10.11 ppm) and selenium (-7.10 to -8.39 ppm) SWHNBs, except that their values are slightly more negative.

Although the trend is reversed, the NICS_{MC}(0)

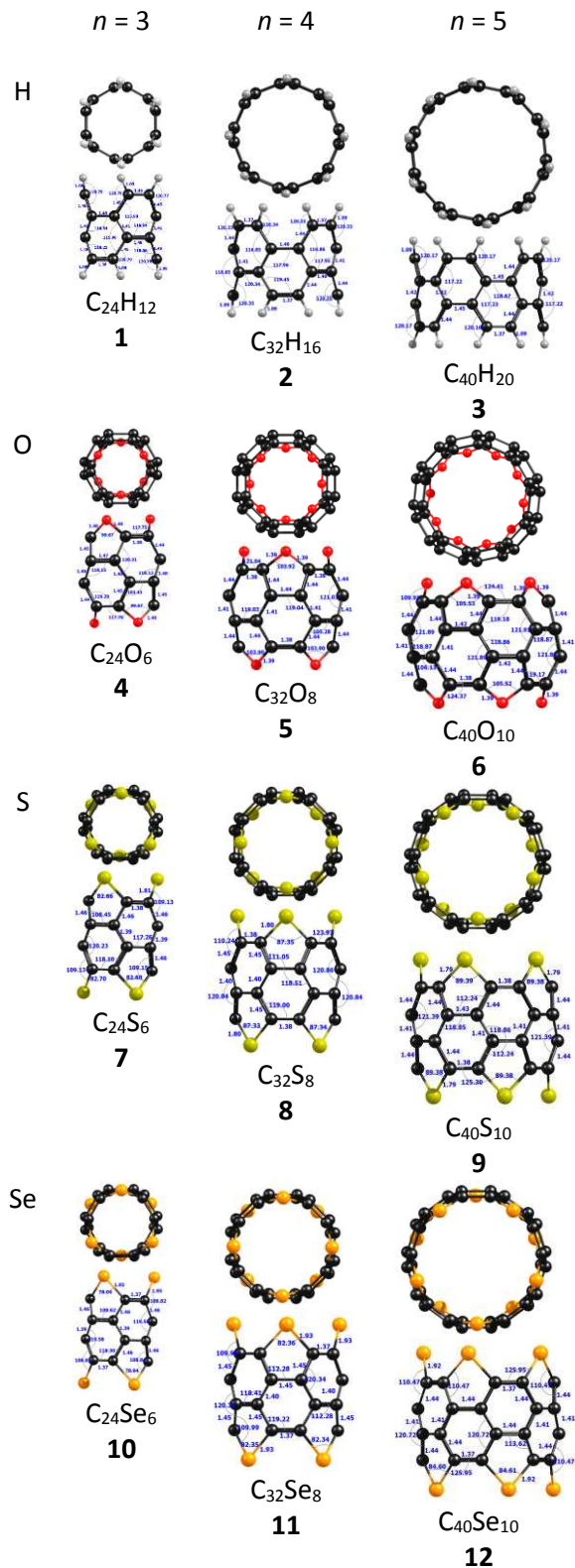


Figure 4. Structures viewed along and parallel to the molecular axis, with selected bond lengths and angles; coloured black=C, red=O, yellow=S and orange=Se.

values for the oxygen derivatives are the most negative out of all the structures. The smallest oxygen derivative **4** is -12.97 ppm, while the largest **6** is -8.52 ppm, which implies that the first three in the oxygen series of SWHNBS are strongly aromatic, although larger derivatives may be less so. For the unsubstituted 'hydrogen', the sulfur and the selenium series, an equal number of paired electrons are added with each additional repeat unit n , so the net effect is an increase in the diatropic ring current (more negative NICS), hence an increase in aromaticity. Interestingly Baryshnikov and co-workers³⁴ found the Sulflower and its heteroatomic analogues to be highly antiaromatic, in stark contrast to the strong aromatic nature of the SWHNBS studied here.

Magnetic susceptibility exaltations^{31,58,59} were used as an additional and complementary technique to NICS. Similarly, large and negative exaltations for molecules are considered to be aromatic while positive values indicate antiaromaticity. For SWCNB compounds **1** and **2**, their exaltations are -84.81 ppm and -60.92 ppm respectively, and while their NICS(0) are 2.36 and -4.43 ppm respectively, these can be inferred as weakly aromatic; the exaltation calculations for **3** could not be completed after multiple attempts. For the SWHNBS, no discernible trend in the exaltations can be deduced, other than that they are significantly more negative, by two or three times those of the SWCNBs, which suggests that the heteroatoms stabilise and induce diatropic ring currents.

The aromaticities were further probed with the vibrational wave number of the aromatic C=C stretch. The vibration shifts to longer wavenumber as each derivative increases in size. For example, the vibration in the SWCNBs shift from 1595.7 cm⁻¹ in **1** ($n=3$) to 1634.9 cm⁻¹ in **3** ($n=5$), and similarly from **7** (1497.3 cm⁻¹) to **9** (1558.7 cm⁻¹). The aromatic C=C stretch all SWHNBS are around ~100 cm⁻¹ less than their

Table 1. Aromaticity calculations.

Entry	NICS _{MC} (0)/ ppm	Λ/ cgs.ppm	C=C/ cm ⁻¹
1	2.36	-84.81	1595.7
2	-4.43	-60.92	1620.9
3	-5.82	*	1634.9
4	-12.97	-147.08	1497.3
5	-10.27	-139.37	1543.7
6	-8.52	-178.15	1558.7
7	-8.77	-186.34	1437.1
8	-10.17	-194.95	1461.0
9	-10.11	-164.24	1466.6
10	-7.10	-142.71	1461.0
11	-8.35	-136.00	1485.3
12	-8.39	-386.08	1487.9

*No exaltation value after multiple attempts.

parent SWCNB counterparts. These observations correlate with the increasingly negative NICS values for each derivative.

In addition to the NICS_{MC}(0) calculated at the centre of each molecule, NICS_{RC}(0) were calculated at the centre of each six-membered carbon ring in the phenacene belt, for the smallest ($n = 3$) compounds in each series (Table 2). The negative NICS_{RC}(0) values for each benzene ring shows that there is a continuous diatropic current around the phenacene belts of each molecule. There is a small difference between the rings around the phenacene belt but all of which are negative and are the same order of magnitude. As a result, there is no distinction between any π -sextets in adjacent rings. So rather than Clar like structures, these SWHNBS appear to be strongly-conjugated Kekulé structures.

Interestingly, the local NICS_{RC}(0) for the individual benzene rings in **1** are on average -1.00 ppm, while the global NICS_{MC}(0) is positive at 2.36 ppm. The benzene rings, therefore, only slightly contribute to the aromaticity. In the SWHNBS, the NICS_{RC}(0) for the benzene rings are significantly more negative, although not as much as the global NICS_{MC}(0).

Table 2. Ring-centred NICS_{RC}(0) isotropic shifts for the benzene rings.

Entry	NICS _{RC} (0) / ppm					
	Ring 1C ₆	Ring 2C ₆	Ring 3C ₆	Ring 4C ₆	Ring 5C ₆	Ring 6C ₆
1	-0.97	-1.07	-1.05	-0.97	-1.07	-1.05
4	-10.96	-11.04	-11.04	-10.96	-11.04	-11.04
7	-7.44	-7.52	-7.44	-7.47	-7.50	-7.46
10	-6.58	-6.50	-6.58	-6.58	-6.50	-6.58

The heteroatoms must therefore provide highly stabilising diatropic contributions. A thorough and exact dissection of σ and π orbital contributions is possible with the MO-NICS technique⁶⁰ but only with planar molecules, while for non-planar structures this analysis is qualitative only³¹ and thus not pursued.

Next, the Frontier Molecular Orbitals (FMO) energy levels were investigated. The highest occupied molecular orbital (HOMO) and lowest unoccupied molecular orbital (LUMO) energy levels are illustrated in Figure 5, along with the corresponding HOMO-LUMO energy gaps (E_g) in electron volts (eV); the work function of a gold electrode⁶¹ is presented for comparison of energy overlap with the HOMO levels of the nanobelts. For the SWCNBs **1-3**, the HOMO level decreases in energy with increasing size, from -4.74 eV to -5.19 eV, while the LUMO energy slightly rises from -2.48 to -2.22 eV. As a result, the E_g increases and therefore the molecules become more stable as they increase in size. Moreover, the HOMO energies correlate well with Itami's nanobelt at -4.92 eV, which infers both the SWCNBs and the SWHNBs should be stable in air. More importantly, these structures can be processed into OTFTs under ambient conditions, a significant manufacturing advantage. The HOMO level of the SWHNBs increases with molecular size from $n=3$ to $n=5$ and the deepest energy level is with **4**. The divergence in the E_g trends can be qualitatively discussed in terms of their FMO densities^{44,62,63}. It is clear that from $n=3$ to 5 the overlap of the HOMO molecular orbitals decreases (ESI,

Table 5) around the central phenacene atoms, which become increasingly concentrated towards the heteroatomic substituents (**5,6**; **7,8**; **9,10**) at the terminal edges – similar to short carbon-based zig-zag nanotubes⁶, who's orbitals tend to diverge into an open-shell along the edges. Structure **4** happens to retain continuous orbital overlap in this region. Another observation is the directional change in orbital densities, where for structures **1-3**, the HOMO orbitals extend between the edges of the belts, whereas those of the SWHNBs extend around belt for the same compounds **5,6**; **7,8**; **9,10**. For **7** and **10**, their orbitals are similar to those of **1-3**, suggesting overall molecular size is a design feature to be considered in future materials. This phenomena of the FMOs needs further investigation as to the underlying contributions towards the E_g in later studies.

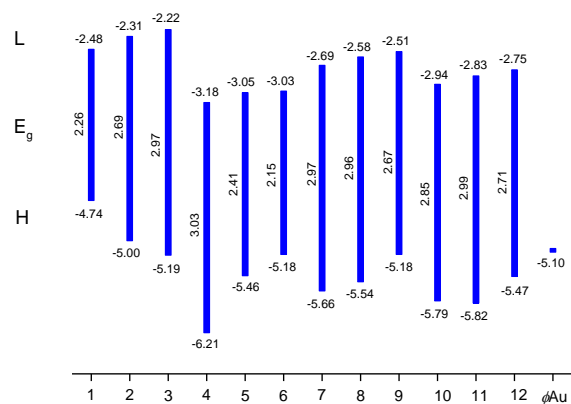
**Figure 5.** HOMO, LUMO and E_g energies (eV) for unsubstituted phenacenes **1-3**, substituted phenacenes **4-12**, and the work function of a gold electrode for comparison.

Table 3. Ionisation potentials and electron affinities *via* DFT (B3LYP), Koopmans' Theorem (KT) and the electron propagator third order pole (P3) with its oscillator strength in parenthesis; DFT values could be acquired for all structures, although KT and P3 proved computationally intractable for several entries (**1**, **5**, **6**, **8**, **9**, **11**, and **12**).

Entry	IE_V			EA_V		
	B3LYP	KT	P3	B3LYP	KT	P3
1	6.20	6.09	6.59 (0.872)	1.08	0.57	0.46 (0.890)
2	6.31	6.26	6.66 (0.863)	1.06	0.66	0.40 (0.883)
3	6.36	-	-	1.09	-	-
4	7.74	8.14	8.60 (0.870)	1.72	0.08	1.06 (0.889)
5	6.83	7.17	7.38 (0.869)	1.72	-	-
6	6.42	6.76	6.94 (0.862)	1.81	-	-
7	7.13	7.50	8.03 (0.873)	1.74	0.29	1.22 (0.886)
8	7.01	7.57	7.66 (0.873)	1.74	-	-
9	6.53	7.02	7.15 (0.867)	1.75	-	-
10	7.10	7.36	7.90 (0.875)	1.68	0.05	0.94 (0.890)
11	7.14	7.48	7.97 (0.875)	1.69	-	-
12	6.53	-	-	1.71	-	-

The vertical ionisation potentials and electron affinities were calculated with the B3LYP functional, Koopmans' Theorem (KT) and the electron propagator third-order pole (P3) and presented in Table 3, with the corresponding pole strength in parenthesis. Compound **12** and **3** proved computationally intractable for ionisation potential calculations with KT and P3 methods, while only the electron affinities of compounds **4**, **7** and **10** were computable after multiple attempts. Although P3 is increasingly used due to its superior accuracy²⁰, both DFT and KT were deployed due to their continued wide-spread use in the literature^{49,64}.

There is a general trend of P3 yielding the highest ionisation potentials, while DFT the lowest; there is no particular trend with the electron affinities. However, the P3 potentials show complex behaviour. The ionisations for **4** (8.60 eV), **7** (8.03 eV) and **10** (7.90 eV) decreases between the oxygen and the selenium compounds, but for **5** (7.38 eV), **8** (7.66 eV) and **11** (7.97 eV), the ionisations increase; the same is true for **6** (6.94 eV) and **9** (7.15 eV). The switch in trends

may be due to the competing effects between the electronegativity of the elements and the increasing conjugation of the molecules; where the latter is a stronger contributor to ionisation potentials. The same observation can be made with the B3LYP functional, while KT gives mixed results. The KT values for the electron affinity are all less than 1 eV, while B3LYP and P3 are generally larger.

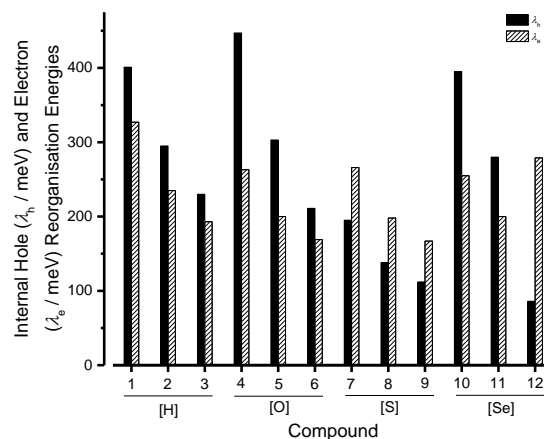


Figure 6. Internal reorganisation hole and electron energies for each compound.

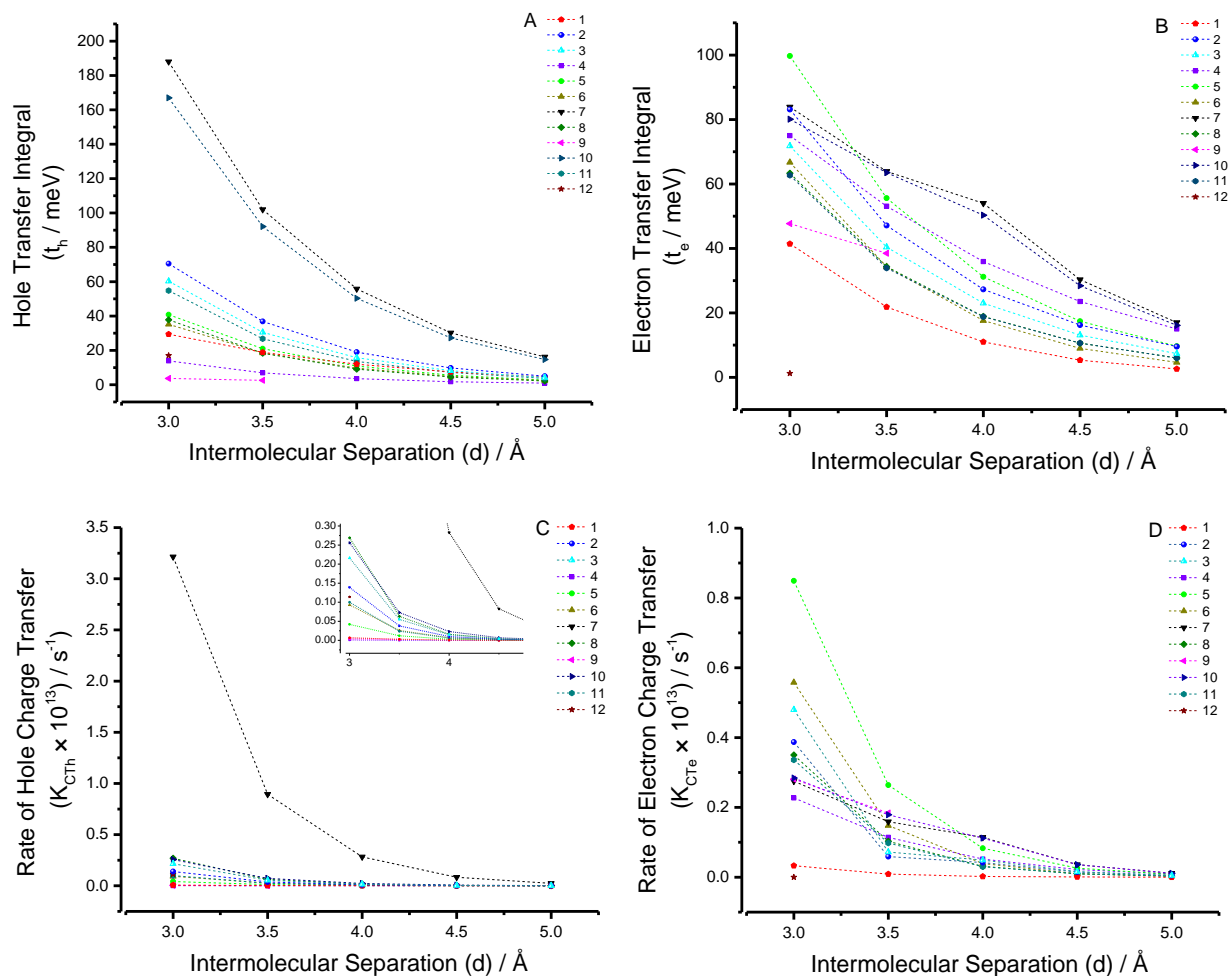


Figure 7. Transfer integrals (A, B) and rates of charge transfer (C, D) for holes and electrons respectively.

The vertical ionisation potentials and electron affinities are the first stage of an electron loss/gain process, as the internal reorganisation energies are the sum totals of the individual relaxation energies of both the neutral and charged states (Figure 6). The hole or electron reorganisation energy of a molecule is the ability for it to mitigate an electron loss or gain respectively; a small value (*ca.* 100-200 meV) is common in high-performing organic semiconductors^{65,66}.

The reorganisation energies for the oxygen and sulfur derivatives show trends similar to each other, while those of selenium are an exception. For example, the hole reorganisation energy decreases from **4-9** (from 447 to 112 meV),

noting that **7** is the lowest out of all $n=3$ compounds at 195 meV, and those of **3** (447 meV) and **10** (395 meV) are relatively similar. This can be explained by the increase in molecular size, as more π -electrons are available and thus electron-electron repulsion is proportionally greater, making the vertical electron loss or gain lower in energy.

The selenium compounds show a spike in the overall decreasing trend, most probably due a decrease in the repulsion between the adjacent selenium atoms as the molecules size increase. The electron reorganisation energies show a general decrease with increasing molecular size, with a small difference between the oxygen and sulfur, and sulfur and selenium derivatives. The

sulfur compounds are more stable towards hole reorganisations and thus more suited to p-type devices than the oxygen and selenium structures.

The second Marcus-Hush parameter, the transfer integral (t), is a measure of the extent of the intermolecular interaction between two molecules that are separated by a distance (d). Combining the integral with the reorganisation energy yields the overall rate of charge transfer (K_{CT}), which is a measure of the efficiency of charge transport between two molecules and thus give a strong indication towards their suitability for electronic materials applications; the charge transfer mobility is calculated using the rate with Equation 10, *vide infra*. The calculated hole and electron integrals are presented in Figure 7; not all intermolecular separations could converge due to the limited interactions between them.

Both the hole transfer integral and the rate of hole charge transfer of the compounds **1** to **3** increases with the size of the molecules, at $d = 3.0$ Å. Although the rate sharply decreases with increasing d , there is still some non-zero hole integral (5.03 meV) at the largest separation $d = 5.0$ Å, inferring sufficient through-space dimer interaction for charge transfer. Compounds **7** and **10** have the largest hole integrals and rates of charge transfer in comparison to the other compounds. Interestingly, **10** has a relatively high hole reorganisation energy (400 meV) but still gives a hole transfer integral of 92.1 meV at $d = 3.5$ Å, similar to that of **7** with 102 meV but has half the reorganisation energy of 200 meV. Compound **4** has equally high reorganisation energies (450 meV), but low hole transfer integral and associated rate of hole charge transfer across all separations. The largest rates of hole and electron charge transfer are with **7** and **5** at $3.215 \times 10^{13} \text{ s}^{-1}$ and $0.849 \times 10^{13} \text{ s}^{-1}$ respectively.

The integrals and rates of electron charge transfer show similar trends to those of the hole parameters, but with noticeable differences. For example, **7** and **10** remain leading compounds at $d = 4.0$ Å, compounds **4** and **5** are close contenders with electron rates of transfer at $0.054 \times 10^{13} \text{ s}^{-1}$ and $0.083 \times 10^{13} \text{ s}^{-1}$ respectively. The rates of **5** and **6** at $d = 3.0$ Å are $0.849 \times 10^{13} \text{ s}^{-1}$ and $0.551 \times 10^{13} \text{ s}^{-1}$ respectively, but fall off drastically with increasing separation. All of the derivatives depreciate between the range $d = 3.0$ - 5.0 Å, but **7** is noticeably the best for both the hole integral and the rate of hole charge transfer. **10** is relatively high performing for the hole integral, but not for the overall rate.

Next, the hole and electron mobilities were

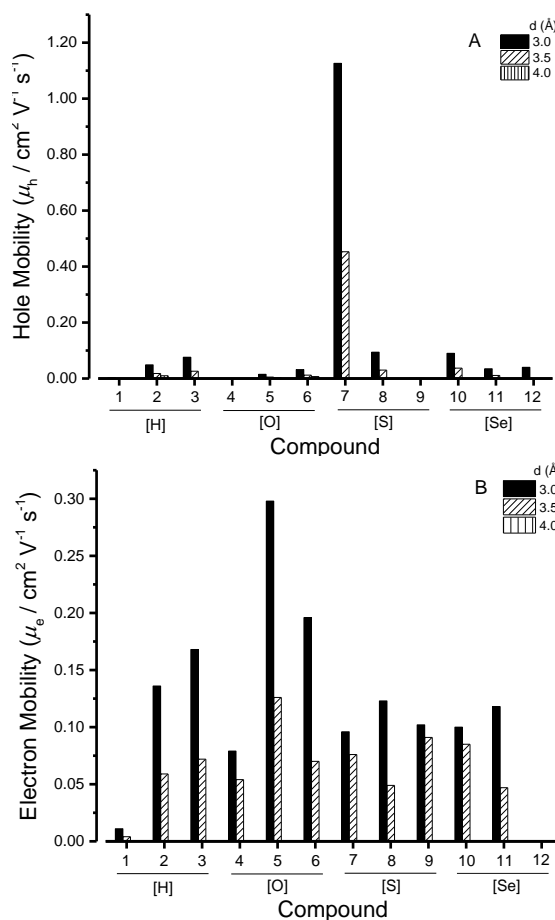


Figure 8. Calculated hole (A) and electron (B) mobilities for compounds **1-12**.

calculated *via* the Einstein-Smoluchowski relationship (Equation 10)²⁹ and presented in Figure 8. Compound **7** has the greatest hole mobility ($1.126 \text{ cm}^2 \text{ V}^{-1} \text{ s}^{-1}$), while all other structures have relatively low values.

Compounds **5** and **6** have the largest electron mobilities, while those of the sulfur and selenium derivatives are lower and similar to each other; **12** has negligible mobilities. Overall, all compounds show promise for electron mobility devices, but only **7** is suitable for hole-based devices.

In reality, the formation of discrete carbon nanobelts is a challenging synthetic task, especially on a scale suitable for widespread applications such as semiconducting materials. However, advances in the formation of the structurally related carbon nanoribbons could be exploited. In recent years, researchers have advanced the stepwise formation of bespoke molecular species in solution⁶⁷ and on surfaces to form all carbon, zig-zag nanoribbons⁶⁸, and used both thermal and electron beam initiated polymerisation reactions of simple molecular precursors in carbon nanotube templates to form armchair carbon and zig-zag heteroatom terminated (S and Cl) nanoribbons^{18,69–71}. Thus, it is envisaged that a similar synthetic approach could be adopted to form the structurally analogous belt-like molecules. This could be achieved by exploiting the self-coupling of a predesigned molecular species under high dilution to give the nanobelts in relative high purity. Or using a more scalable, self-assembly approach involving the polymerisation of molecular fragments within an appropriately suitably shaped template or nanoreactor. The size of the nanobelts could be controlled by sequential addition of the building blocks within the initial precursor species or *via* careful section of the template used respectively.

Conclusion

This study has investigated the structural and energetic properties of the compounds generated from the heteroatomic substituents into the chair-positions of the phenacene-based SWCNBs, yielding a small and novel virtual library of SWHNBs. These structures were theoretically screened for potential applications in organic electronics. It is clear that a small number have relatively large FMO energy gaps, sufficient to suggest air-stability by comparison to recently synthesised structures, as well as excellent ionisations. One compound was found to have a hole mobility exceeding $1 \text{ cm}^2 \text{ V}^{-1} \text{ s}^{-1}$, even though the SWCNBs are two orders of magnitude less. This approach highlights (i) that the heteroatoms within the structure stabilise the nanobelts and (ii) that theoretical calculations are a powerful way of evaluating new materials and directing experimental endeavours. This study sets out design rules for 3D organic semiconductors highlighting potential candidates for the next generation of carbon nanomaterials-based semiconductor systems.

Acknowledgements

We are thankful to the Gunnell and Mathews Scholarship for funding and the Advanced Computing Research (ARC) 2 and 3 facilities at the University of Leeds for computational resources.

References

- 1 G. Povie, Y. Segawa, T. Nishihara, Y. Miyauchi and K. Itami, *Science*, 2017, **356**, 172–175.
- 2 C. Zhou, J. Kong and H. Dai, *Phys. Rev. Lett.*, 2000, **84**, 5604–5607.
- 3 V. H. Crespi, M. L. Cohen and A. Rubio, *Phys. Rev. Lett.*, 1997, **79**, 2093–2096.
- 4 M. J. O’Connell, S. M. Bachilo, C. B.

- Huffman, V. C. Moore, M. S. Strano, E. H. Haroz, K. L. Rialon, P. J. Boul, W. H. Noon, C. Kittrell, J. Ma, R. H. Hauge, R. B. Weisman and R. E. Smalley, *Science*, 2002, **297**, 593–6.
- 5 M. Bendikov, H. M. Duong, K. Starkey, K. N. Houk, E. A. Carter and F. Wudl, *J. Am. Chem. Soc.*, 2004, **126**, 7416–7417.
- 6 Z. Chen, D. Jiang, X. Lu, H. F. Bettinger, S. Dai, P. von R. Schleyer and K. N. Houk, *Org. Lett.*, 2007, **9**, 5449–5452.
- 7 H. Takato, K. Sunouchi, N. Okabe, A. Nitayama, K. Hieda, F. Horiguchi and F. Masuoka, *IEEE Trans. Electron Devices*, 1991, **38**, 573–578.
- 8 S. Kobayashi, T. Nishikawa, T. Takenobu, S. Mori, T. Shimoda, T. Mitani, H. Shimotani, N. Yoshimoto, S. Ogawa and Y. Iwasa, *Nat. Mater.*, 2004, **3**, 317–322.
- 9 S. J. Kang, C. Kocabas, T. Ozel, M. Shim, N. Pimparkar, M. A. Alam, S. V. Rotkin and J. A. Rogers, *Nat. Nanotechnol.*, 2007, **2**, 230–236.
- 10 F. Patolsky, B. P. Timko, G. Yu, Y. Fang, A. B. Greytak, G. Zheng and C. M. Lieber, *Science*, 2006, **313**, 1100–4.
- 11 H. A. Wegner, *Angew. Chemie - Int. Ed.*, 2017, **56**, 10995–10996.
- 12 J. S. Siegel, *Science (80-)*, 2017, **356**, 135–136.
- 13 A. Robert, P. Dechambenoit, E. A. Hillard, H. Bock and F. Durola, *Chem. Commun.*, 2017, **53**, 11540–11543.
- 14 N. Oldani, S. K. Doorn, S. Tretiak and S. Fernandez-Alberti, *Phys. Chem. Chem. Phys.*, 2017, **19**, 30914–30924.
- 15 S.-Z. Zeng, X. Zeng, W. Tu, Y. Yao, L. Yu, H. Wu, W. Jin, H. Huang and J. Zou, *J. Mater. Chem. A*, 2017, **5**, 23209–23220.
- 16 T. Ouyang, K. Cheng, F. Yang, L. Zhou, K. Zhu, K. Ye, G. Wang and D. Cao, *J. Mater. Chem. A*, 2017, **5**, 14551–14561.
- 17 J. T. Han, J. I. Jang, J. Y. Cho, J. Y. Hwang, J. S. Woo, H. J. Jeong, S. Y. Jeong, S. H. Seo and G.-W. Lee, *Sci. Rep.*, 2017, **7**, 4931.
- 18 A. Chuvilin, E. Bichoutskaia, M. C. Gimenez-Lopez, T. W. Chamberlain, G. A. Rance, N. Kuganathan, J. Biskupek, U. Kaiser and A. N. Khlobystov, *Nat. Mater.*, 2011, **10**, 687–692.
- 19 T. Qi, W. Qiu, Y. Liu, H. Zhang, X. Gao, Y. Liu, K. Lu, C. Du, G. Yu and D. Zhu, *J. Org. Chem.*, 2008, **73**, 4638–4643.
- 20 L. Jones and L. Lin, *Comput. Theor. Chem.*, 2017, **1115**, 22–29.
- 21 C. K. Yong, A. J. Musser, S. L. Bayliss, S. Lukman, H. Tamura, O. Bubnova, R. K. Hallani, A. Meneau, R. Resel, M. Maruyama, S. Hotta, L. M. Herz, D. Beljonne, J. E. Anthony, J. Clark and H. Sirringhaus, *Nat. Commun.*, , DOI:10.1038/ncomms15953.
- 22 W. Jiang, Y. Li and Z. Wang, *Chem. Soc. Rev.*, 2013, **42**, 6113–27.
- 23 J. E. Anthony, *Chem. Rev.*, 2006, **106**, 5028–5048.
- 24 A. Dadvand, F. Cicoira, K. Y. Chernichenko, E. S. Balenkova, R. M. Osuna, F. Rosei, V. G. Nenajdenko and D. F. Perepichka, *Chem. Commun.*, 2008, 5354.
- 25 K. Y. Chernichenko, V. V. Sumerin, R. V. Shpanchenko, E. S. Balenkova and V. G. Nenajdenko, *Angew. Chemie Int. Ed.*, 2006, **45**, 7367–7370.
- 26 M. D. Hanwell, D. E. Curtis, D. C. Lonie, T. Vandermeersch, E. Zurek and G. R. Hutchison, *J. Cheminform.*, 2012, **4**, 17.
- 27 J. C. Sancho-García and A. J. Pérez-Jiménez, *Phys. Chem. Chem. Phys.*, 2009, **11**, 2741–2746.

- 28 G. Mallocci, G. Mulas, G. Cappellini and C. Joblin, *Chem. Phys.*, 2007, **340**, 43–58.
- 29 G. Cappellini, G. Mallocci and G. Mulas, *Superlattices Microstruct.*, 2009, **46**, 14–18.
- 30 M. J. Frisch, G. W. Trucks, H. B. Schlegel, G. E. Scuseria, M. A. Robb, J. R. Cheeseman, G. Scalmani, V. Barone, G. A. Petersson, H. Nakatsuji, X. Li, M. Caricato, A. Marenich, J. Bloino, B. G. Janesko, R. Gomperts, B. Mennucci, H. P. Hratchian, J. V. Ortiz, A. F. Izmaylov, J. L. Sonnenberg, D. Williams-Young, F. Ding, F. Lipparini, F. Egidi, J. Goings, B. Peng, A. Petrone, T. Henderson, D. Ranasinghe, V. G. Zakrzewski, J. Gao, N. Rega, G. Zheng, W. Liang, M. Hada, M. Ehara, K. Toyota, R. Fukuda, J. Hasegawa, M. Ishida, T. Nakajima, Y. Honda, O. Kitao, H. Nakai, T. Vreven, K. Throssell, J. A. Montgomery, J. E. P. Jr., F. Ogliaro, M. Bearpark, J. J. Heyd, E. Brothers, K. N. Kudin, V. N. Staroverov, T. Keith, R. Kobayashi, J. Normand, K. Raghavachari, A. Rendell, J. C. Burant, S. S. Iyengar, J. Tomasi, M. Cossi, J. M. Millam, M. Klene, C. Adamo, R. Cammi, J. W. Ochterski, R. L. Martin, K. Morokuma, O. Farkas, J. B. Foresman, D. J. Fox, Gaussian, Inc. and Wallingford, 2016.
- 31 C. Zhongfang, W. Chaitanya S., C. Clmence, P. Ralph and von R. S. Paul, *Chem. Rev.*, 2005, **105**, 3842–3888.
- 32 A. Stanger, *J. Org. Chem.*, 2006, **71**, 883–893.
- 33 G. Monaco and R. Zanasi, *J. Phys. Chem. Lett.*, 2017, **8**, 4673–4678.
- 34 G. V. Baryshnikov, R. R. Valiev, N. N. Karaush and B. F. Minaev, *Phys. Chem. Chem. Phys.*, 2014, **16**, 15367.
- 35 M. B??hl and A. Hirsch, *Spherical aromaticity of fullerenes*, 2001, vol. 101.
- 36 W. E. Billups, A. Gonzalez, C. Gesenberg, W. Luo, T. Marriott, L. B. Alemany, M. Saunders, H. A. Jiménez-Vázquez and A. Khong, *Tetrahedron Lett.*, 1997, **38**, 175–178.
- 37 R. C. Haddon, *Nature*, 1995, **378**, 249–255.
- 38 R. C. Haddon, L. F. Schneemeyer, J. V. Waszczak, S. H. Glarum, R. Tycko, G. Dabbagh, A. R. Kortan, A. J. Muller, A. M. Mujsce, M. J. Rosseinsky, S. M. Zahurak, A. V. Makhija, F. A. Thiel, K. Raghavachari, E. Cockayne and V. Elser, *Nature*, 1991, **350**, 46–47.
- 39 S. Refaely-Abramson, R. Baer and L. Kronik, *Phys. Rev. B*, 2011, **84**, 75144.
- 40 P. Sjoberg, J. S. Murray, T. Brinck and P. Politzer, *Can. J. Chem.*, 1990, **68**, 1440–1443.
- 41 T. Koopmans, *Physica*, 1934, **1**, 104–113.
- 42 D. Danovich, *Wiley Interdiscip. Rev. Comput. Mol. Sci.*, 2011, **1**, 377–387.
- 43 O. Dolgounitcheva, M. Díaz-Tinoco, V. G. Zakrzewski, R. M. Richard, N. Marom, C. D. Sherrill and J. V. Ortiz, *J. Chem. Theory Comput.*, 2016, **12**, 627–637.
- 44 M. Winkler and K. N. Houk, *J. Am. Chem. Soc.*, 2007, **129**, 1805–1815.
- 45 G. R. Hutchison, M. A. Ratner and T. J. Marks, *J. Am. Chem. Soc.*, 2005, **127**, 2339–2350.
- 46 C. R. Newman, C. D. Frisbie, D. A. da S. Filho, J.-L. Brédas, P. C. Ewbank and K. R. Mann, *Chem. Mater.*, 2004, **16**, 4436–4451.
- 47 B. Baumeier, J. Kirkpatrick and D. Andrienko, *Phys. Chem. Chem. Phys.*, 2010, **12**, 11103–11113.
- 48 J. C. Sancho-García and A. J. Pérez-Jiménez, *Chem. Phys. Lett.*, 2010, **499**, 146–151.

- 49 R. Cardia, G. Mallocci, A. Bosin, G. Serra and G. Cappellini, *Chem. Phys.*, 2016, **478**, 8–13.
- 50 S. C. B. Mannsfeld, A. Virkar, C. Reese, M. F. Toney and Z. Bao, *Adv. Mater.*, 2009, **21**, 2294–2298.
- 51 G. Likhtenshtein, *Solar energy conversion : chemical aspects; electron transfer theories*, Wiley-VCH, 2012.
- 52 O. Hammerich and B. Speiser, Eds., *Organic Electrochemistry, Fifth Edition*, CRC Press, 2015.
- 53 A. C. Benniston, A. Harriman, H. Tsue, S. Higashida, T. Akiyama, E. Yoshizawa, M. Aoki, K. Yamada, K. Hagiwara, S. Taniguchi and T. Okada, *Chem. Soc. Rev.*, 2006, **35**, 169–179.
- 54 Z. Shuai, H. Geng, W. Xu, Y. Liao, J.-M. André, H. Geng, C. A. Di, W. P. Hu, Z. G. Shuai, K. Singh and D. B. Zhu, *Chem. Soc. Rev.*, 2014, **43**, 2662.
- 55 L. Wang, G. Nan, X. Yang, Q. Peng, Q. Li, Z. Shuai, J. S. Tan, R. G. Della Valle, E. Venuti, J. Jose, S. R. Gadre, G. R. Desiraju, T. S. Thakur, B. P. van Eijck, J. C. Facelli, V. E. Bazterra, M. B. Ferraro, D. W. M. Hofmann, M. A. Neumann, F. J. J. Leusen, J. Kendrick, S. L. Price, A. J. Misqutta, P. G. Karamertzanis, G. W. A. Welch, H. A. Scheraga, Y. A. Arnautova, M. U. Schmidt, J. van de Streek, A. K. Wolf and B. Schweizer, *Chem. Soc. Rev.*, 2010, **39**, 423–434.
- 56 V. Coropceanu, H. Li, P. Winget, L. Zhu and J.-L. Brédas, *Annu. Rev. Mater. Res.*, 2013, **43**, 63–87.
- 57 G. Mallocci, G. Cappellini, G. Mulas and A. Mattoni, *Chem. Phys.*, 2011, **384**, 19–27.
- 58 H. J. Dauben, J. D. Wilson and J. L. Laity, *J. Am. Chem. Soc.*, 1968, **90**, 811–813.
- 59 P. v. R. Schleyer, H. Jiao, M. N. Glukhovtsev, J. Chandrasekhar and E. Kraka, *J. Am. Chem. Soc.*, 1994, **116**, 10129–10134.
- 60 T. Heine, P. v. R. Schleyer, C. Corminboeuf, G. Seifert, R. Reviakine and J. Weber, 2003, **107**, 6470–6475.
- 61 K. W. J. Heard, J. J. Morrison, L. Weston, C. H. Lo, L. Pirvu, J. Raftery, M. S. Little, J. J. W. McDouall, S. G. Yeates and P. Quayle, *Chem. Commun.*, 2015, **51**, 6115–6118.
- 62 T. P. Nguyen, J. H. Shim and J. Y. Lee, *J. Phys. Chem. C*, 2015, **119**, 11301–11310.
- 63 V. T. T. Huong, T. B. Tai and M. T. Nguyen, *Phys. Chem. Chem. Phys.*, 2012, **14**, 14832–14841.
- 64 L. Jones and L. Lin, *J. Phys. Chem. A*, 2017, **121**, 2804–2813.
- 65 H. Xia, D. Liu, X. Xu, Q. Miao, J.-L. Brédas, K. Matsumoto, H. Kurata, T. Kubo, S. Shinamura, H. Mori, E. Miyazaki and K. Takimiya, *Chem. Commun.*, 2013, **49**, 4301–4303.
- 66 J.-L. Brédas, D. Beljonne, V. Coropceanu and J. Cornil, *Chem. Rev.*, 2004, **104**, 4971–5004.
- 67 T. H. Vo, M. Shekhiriev, D. A. Kunkel, F. Orange, M. J.-F. Guinel, A. Enders and A. Sinitskii, *Chem. Commun.*, 2014, **50**, 4172–4174.
- 68 P. Ruffieux, S. Wang, B. Yang, C. Sánchez-Sánchez, J. Liu, T. Dienel, L. Talirz, P. Shinde, C. A. Pignedoli, D. Passerone, T. Dumslaff, X. Feng, K. Müllen and R. Fasel, *Nature*, 2016, **531**, 489–492.
- 69 A. V. Talyzin, I. V. Anoshkin, A. V. Krashenninnikov, R. M. Nieminen, A. G. Nasibulin, H. Jiang and E. I. Kauppinen, *Nano Lett.*, 2011, **11**, 4352–4356.
- 70 T. W. Chamberlain, J. Biskupek, S. T. Skowron, A. V. Markevich, S. Kurasch, O. Reimer, K. E. Walker, G. A. Rance, X.

Feng, K. Müllen, A. Turchanin, M. A. Lebedeva, A. G. Majouga, V. G. Nenajdenko, U. Kaiser, E. Besley and A. N. Khlobystov, *ACS Nano*, 2017, **11**, 2509–2520.

71 T. W. Chamberlain, J. Biskupek, G. A. Rance, A. Chuvilin, T. J. Alexander, E.

Bichoutskaia, U. Kaiser and A. N. Khlobystov, *ACS Nano*, 2012, **6**, 3943–3953.